Design Evaluation and Numerical Study of Micro-Heating for a Microfluidic Loop-Mediated Isothermal Amplification

Deni Haryadi
Department of Mechanical Engineering, Faculty of Engineering, Universitas Indonesia

Hashfi Abidi
Department of Mechanical Engineering, Faculty of Engineering, Universitas Indonesia

Jos Istiyanto
Department of Mechanical Engineering, Faculty of Engineering, Universitas Indonesia

Yudan Whulanza
Department of Mechanical Engineering, Faculty of Engineering, Universitas Indonesia

他

https://doi.org/10.5109/7326970

Design Evaluation and Numerical Study of Micro-Heating for a Microfluidic Loop-Mediated Isothermal Amplification

Deni Haryadi[1,2], Hashfi Abidi[1], Jos Istiyanto[1], Yudan Whulanza[1,3,*], Nilo T. Bugtai[4]

[1]Department of Mechanical Engineering, Faculty of Engineering, Universitas Indonesia, Depok, Indonesia
[2]Department of Mechanical Engineering, Faculty of Engineering, Gunadarma University, Depok, Indonesia
[3]Research Center for Biomedical Engineering, Universitas Indonesia, Indonesia
[4]De La Salle University, 2401 Taft Avenue, 0922, Manila, Philippines

*Author to whom correspondence should be addressed:
E-mail: yudan.whulanza@ui.ac.id

(Received February 3, 2024; Revised June 28, 2024; Accepted November 25, 2024).

Abstract: The emergence of COVID-19 highlighted the urgent need for rapid and accurate diagnostic tools. Loop-mediated isothermal amplification (LAMP) has gained significant attention for its rapidity, simplicity, and cost-effectiveness, especially for point-of-care testing. However, precise and uniform temperature control in micro-heating systems remains challenging, limiting the portability of conventional LAMP assays. This study addresses these challenges by designing and simulating a micro-heater optimized for low power consumption and high temperature uniformity. Utilizing multiphysics simulation software, we modeled the heating element with variable voltage differences to achieve the precise temperature distribution required for LAMP processes. Our results show that at a voltage of 0.3V, the micro-heater achieved temperatures of 41°C in 1 minute and 51°C in 60 minutes, closely matching simulation predictions. The microfluidic device successfully integrated the micro-heater, achieving uniform temperature distribution with minimal variation of 1.5°C across the chip. Experimental validation confirmed the micro-heater's effectiveness, demonstrating rapid and uniform heating with low power consumption. These findings enhance the reliability and efficiency of LAMP-based assays, making the design suitable for portable diagnostic tools. This innovation is crucial for developing cost-effective diagnostic tools for resource-limited settings, contributing significantly to efficient disease management and surveillance.

Keywords: LAMP; Micro Heater; Miniaturization; Heat Transfer Simulation

1. Introduction

In the early months of 2020, the world was confronted with an unprecedented and rapidly spreading outbreak known as COVID-19. Caused by the novel coronavirus SARS-CoV-2, this infectious disease was first identified in the city of Wuhan, China In a matter of weeks, the virus transcended geographical boundaries, affecting populations worldwide and leading to a global pandemic[1-2)]. The rapid spread and the severe impact of COVID-19 underscored the vulnerability of global health systems to novel pathogens and the importance of timely and accurate diagnostic tools in managing such outbreaks. The COVID-19 pandemic has highlighted the crucial role of Polymerase Chain Reaction (PCR) technology in managing virus spread and diagnosing infections. PCR has emerged as a primary tool for identifying and confirming the presence of the Coronavirus (SARS-CoV-2) in human samples[3-5)].

PCR is a powerful molecular biology technique that allows scientists to amplify specific segments of DNA or RNA[6)]. In the context of COVID-19, PCR is used to detect the genetic material of the SARS-CoV-2 virus in clinical samples, such as nasopharyngeal swabs or throat swabs[7)]. The detection of the virus's genetic material is a critical step in diagnosing COVID-19 infections. One of the main challenges of the conventional PCR method is the time required to complete the DNA amplification process. Conventional PCR method takes several hours to finish the amplification cycles, which can slow down analysis and diagnosis. Additionally, conventional PCR also requires a relatively large reaction volume, which often becomes impractical for applications where the available sample is limited[8-9)]. To address these limitations, research in the field of micro-LAMP has become a primary focus in the development of LAMP technology[10-12)]. Micro LAMP involves the miniaturization of LAMP reactions into microfluidic devices, enabling the use of very small

reaction volumes (usually a few microliters) and short amplification times (in minutes). Increasing the efficiency of the heater will certainly affect the performance of the Micro-LAMP system[13-15].

To begin, the micro heater's design and material play a significant role in enabling low power consumption, low thermal mass, effective temperature homogeneity across the device, and increased thermal insulation from the surrounding environment[16-18]. Second, the stability of the heater under ambient conditions is one of the most important variables that determines the longevity, reusability, and application of the micro heater in surroundings that are unstable[19-21]. Lastly, a wide use of microheater need a certain consideration from the design and also the fabrication. There are application in sensors[22-24], actuators[25-26], and also biomedical application such as cell culture, bacterial and nucleic acid sensing[27-29].

In the current study, the design and electro-thermal simulation of micro-heaters that are utilized in a portable DNA amplification system are described in detail[30-31]. The optimization of the design is centered on the goal of obtaining reduced power consumption and increased temperature uniformity. At this point in time, a numerical model of macro heating systems has already been constructed[32-33], however micro to mini scale heating systems are quite uncommon to come across. Simulations of the amount of energy required to ensure that the Loop-mediated isothermal amplification (LAMP) as a heating system is successful with the least amount of heating material and the most effective natural cooling have been carried out using multiphysics software.

2. Methods

2.1 Mathematical Modelling

In the process of analyzing the structure of the microheater, mathematical modeling has proven beneficial in understanding heat transport, device temperature, and determining design variables. The dissipation of heat in microsystems is distinct from that of bulk materials because of the differences in thermal conductivities and heat transfer coefficients that occur at nanoscale thicknesses from bulk materials. Since this is the case, the modeling of heat transfer and power consumption at the microscale will result in a more comprehensive understanding of the performance of the microdevice. The power applied to the micro-heater is represented by:

$$P_{in} = \frac{V_{in}^2}{R} = \frac{V_{in}^2 A}{\rho L} \quad (1)$$

The aforementioned equation pertains to the micro-heater's characteristics, where Vin denotes the voltage applied, R represents the resistance, ρ signifies the resistivity, L denotes the length, and A represents the cross-sectional area. The application of voltage and the determination of equivalent resistance allow for the calculation of the current flowing through the heater in accordance with Ohm's law.

Heat dissipation in the micro-heater is caused by conduction through the underlying layer encompassing the heating element and contact pads, convection towards the surrounding air, and radiation. These factors are accounted for in the following equations.

$$P_{conduction} = \frac{kA_{conduction}[T-T_a]}{L} \quad (2)$$

In this equation, T represents the high temperature that was measured on the heater structure, Ta stands for the temperature of the substrate, and L is the length of the microheater structure. Additionally, the symbol k refers to the thermal conductivity of the micro-heater, which is measured in unit of watts per meter Kelvin. The specific region of heat transfer that is designated by its method of action is referred to as one that is characterized by conduction.

$$A_{conduction} = k_{Pi}A_{pi} + k_{Ag}A_{Ag} \quad (3)$$

where Aag and Api represent the cross-sectional area of the silver layer and kAg and kpi represent the thermal conductivity of the polyimide layer, on the other hand. The power loss that occurs as a result of convection to the air in the surrounding area is controlled by

$$P_{convection} = hA_{surface}[T - T_a] \quad (4)$$

where h can be thought of as the heat transfer coefficient of air and in the context of the heating element, a surface refers to the surface area. It is the Stefan-Boltzmann Law that governs the process of determining the amount of power loss that is caused by radiation sources.

$$P_{radiation} = \sigma\varepsilon A_{surface}[T^4 - T_a^4] \quad (5)$$

where σ represents the Stefan-Boltzmann constant, which is equal to 5.67×10^{-8} Wm^{-2} K^{-4}, and ε represents the emissivity of the surface of the heating element. In conclusion, the absolute amount of power that is lost is established by.

$$P_{disp} = P_{conduction} + P_{convaction} + P_{radiation} \quad (6)$$

2.2 Numerical Simulation using Ansys Software

The modeling of the Joule heating effect is accomplished through the finite element method (FEM) in conjunction with Ansys software. To initiate the simulation, the "Workbench" program must be selected by the user to start the Ansys software. Subsequently,

'Electric' is to be selected from the 'Analysis Systems' in the 'Toolbox' bar as depicted in FIg.1(a).

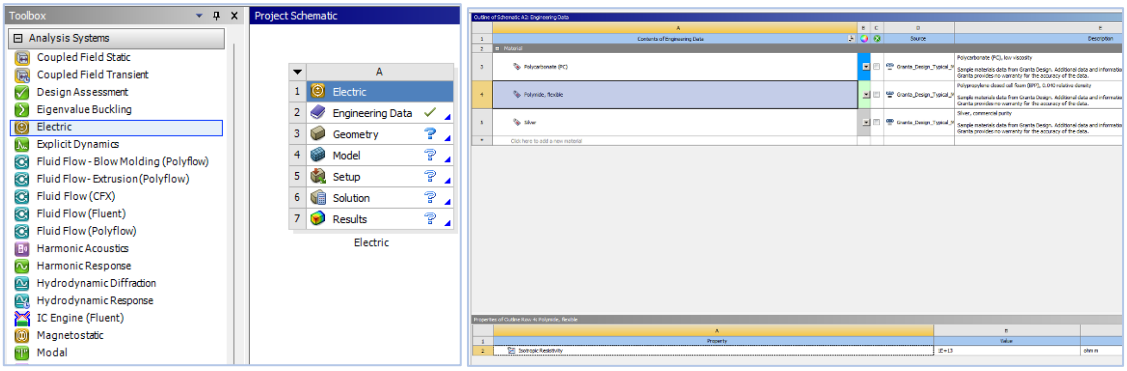

(a) (b)

Fig. 1: (a) the starting dialogue from the software and (b) material selection to be determined in boundary conditions of the numerical study.

Material Selection

Materials required for the simulation are selected and defined in this section Fig. 1(b). The materials are adjusted to each location: a base of polyimide with high resistivity for the body, a mount for the microfluidic chip made of polycarbonate, and silver for the heating electrode. Table 1. Table 1 shows the parameters that were used in this numerical setup.

Table 1. Material properties used in the thermal analysis.

Material	Density (kg/m^3)	Heat capacity C_p ($J/Kg.K^o$)	Thermal conductivity $k(W/m.K^o)$	Electric conductivity (S/m)
Silver/Ag	10,500	0.233	429	61.6×10^6
Polyimide	1,300	1.67	0.06	2.8×10^{-14}
Polycarbonate	12,000	1.2	0.20	8.0×10^{-3}
Water	1,000	4,186	0.606	5.5×10^6

Geometric Model of the Microfluidic system

The microfluidic system designed is based on a commercial chip from Microfluidic Chip shop GmbH with reactor chamber 584 series. (Jena, Jerman). Geometry can be seen in a catalogue that has been published publicly. The overall size is as large as a biological preparate that is then assembled onto a polyimide chip that has been coated with screen printed silver heater. The design process uses Ansys Student Version (Pennsylvania, US) software to create a three-dimensional image of the assembly between the chip and the heating material.

Meshing the Model

Meshing or FEA discretization, which converts a continuous solid domain into a discrete computational domain to enable the solving of structural equations using the FEA numerical method, is described in references[34,35]. Tetrahedral meshing is employed in complex areas such as supports due to its ability to conform to complex geometries. Conversely, in simpler areas, hexahedral meshing is utilized to achieve an efficient mesh with high resolution and computational speed. The mesh sizes average at 0.1 mm, with the smallest size being 0.001 mm, resulting in a mesh comprising approximately 639,444 nodes and 188,570 elements.

Set-Up and Solving the Model

Indicating the direction in which the flow of voltage is directed towards the microfluid heating system is an essential requirement. This system will have its voltage input situated at the bottom of the microfluid chip whenever it is in operation. Fig. 2(a) illustrates the connection of the heating electrode, which is connected to a voltage of approximately one volt.

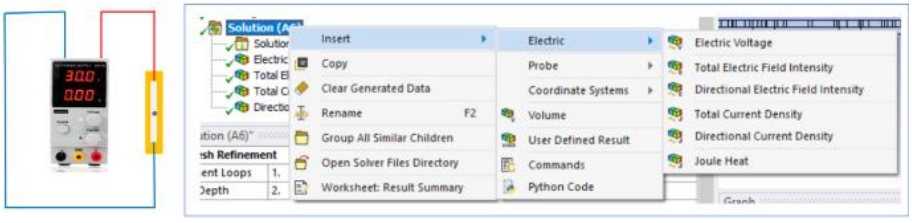

(a) (b)

Fig. 2: (a) Experimental scheme for microfluidic systems during electrification and (b) dialogue box on software to run the electrical flow process on the microfluidic system.

It is vital to explain the nature of the problem that the software is seeking to solve through the simulation. In conclusion, it is essential to specify the nature of the problem. For the purpose of carrying out this mode, the 'Solution' tab was selected, and thereafter, the options 'Insert' and 'Electric' were selected from the list of possibilities that were accessible Fig. 2(b). After that, the 'Electric Voltage' and 'Total Current Density' controls were selected, and the 'Solve' button was brought to the user's attention.

3. Results and Discussions

The designed microfluidic chip, capable of holding a volume of 20 µL, includes a sample inlet and a commercial reactor chip from Microfluidic Chip Shop Fig. 3(a). This commercial chip, as claimed by the manufacturer, can perform generic reactions in micro volumes. The geometrical models used for simulating the proposed design are displayed in Fig. 3(b). A polymeric film, 100 µm in thickness, was integrated into the chip to completely enclose it on both sides, serving as an effective enclosure. Rapid temperature generation from the silver coating on the polymeric film was observed when connected to an electrical source. This silver electrode patterned in the polyimide polymer serves as the micro-heater, as demonstrated in our previous experiments[36,37].

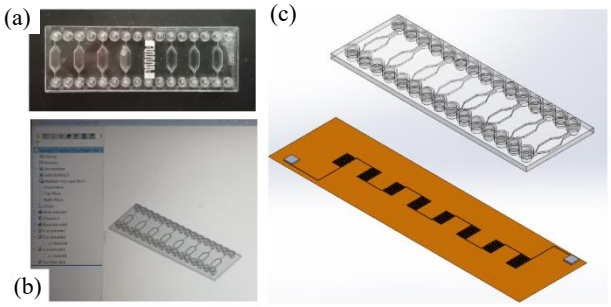

Fig. 3: (a) Commercial chip reactor products from manufacturers; (b) solid model manufacturing process by following size according to product catalogues and (c) assembly of chip reactors with polyimides that have been prepared by heating silver electrode.

Fig. 3(c) depicts a completed section of two components: a microfluidic device containing a micro chamber for amplification, and a polyimide sheet for effective heat transfer to and from the liquid specimen within the micro chamber. An efficient amplification reaction is essential for the successful execution of the Loop-Mediated Isothermal Amplification (LAMP). The amplification typically occurs within the temperature range of 50-90 °C, which serves as the boundary condition for our numerical investigation[38,39].

It is expected that the perfect micro-heater, which operates on the concept of the Joule effect, will be able to achieve the desired temperature level while consuming the least amount of electricity that is feasible. It is the provision of a heater that is required in order for the heating mechanism of the platform shown in Fig. 4(a) to function properly. The power source initiates the flow of an electric current within the heater, which ultimately results in an increase in the thermal energy that is contained within the heater.

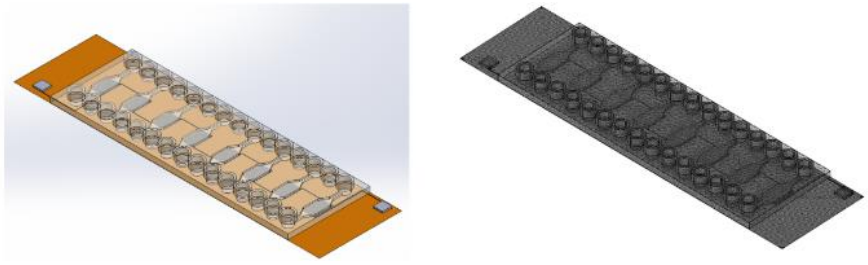

(a) (b)

Fig. 4: (a) Complete models of microfluidic systems for LAMP and (b) meshing results according to the methods mentioned.

A representation of the mesh that will be utilized in the execution of the simulation can be found in Fig. 4(b). The initial temperature is twenty degrees Celsius, and it will continue to rise from there. The surfaces that are next to the border are simultaneously subjected to the application of convective cooling. The model is finally computed in order to produce a result that is reliant on the passage of time. With voltages of 0.1 V, 0.3 V, 0.6 V, 0.8 V, and 1V, the simulation of the Joule heating effect will be carried out for a period of time ranging from 0 to 60 minutes. At the same time, the simulation will be carried out.

The response time of the microheater was observed at a number of different voltages as part of a time-dependent investigation that was carried out for the purpose of design. Fig. 5 depicts the resulted thermal achieved at time span from 0 to 60 minutes for 0.3 V applying voltage. Fig. 5(a) shows the result after 1 minute, while Fig. 5(b) shows the result after 60 minutes. It can be seen that the temperatures

reached are in the range of 40 and 50 for 1 and 60 minutes, respectively.

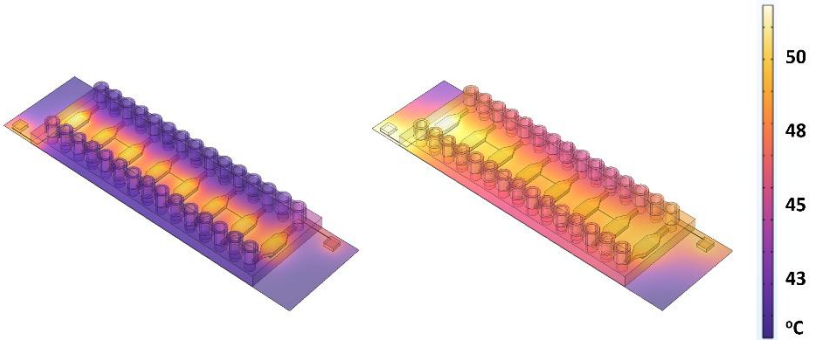

(a) (b)

Fig. 5: (a) The numerical result of the heating process on the microfluidic system for:(a) 1 minute and (b) 60 minutes at applying voltage of 0.3 V.

Figure 6 presents the numerical study results for the heating process with applied voltages ranging from 0.1-1 V. Part (a) depicts the temperature distribution over time within 60 minutes, while part (b) shows the rate of temperature increase for various applied voltage variations. Key observations include the rate of temperature increase, the steady-state temperature achieved, voltage efficiency, and the uniformity of temperature distribution across the heater surface.

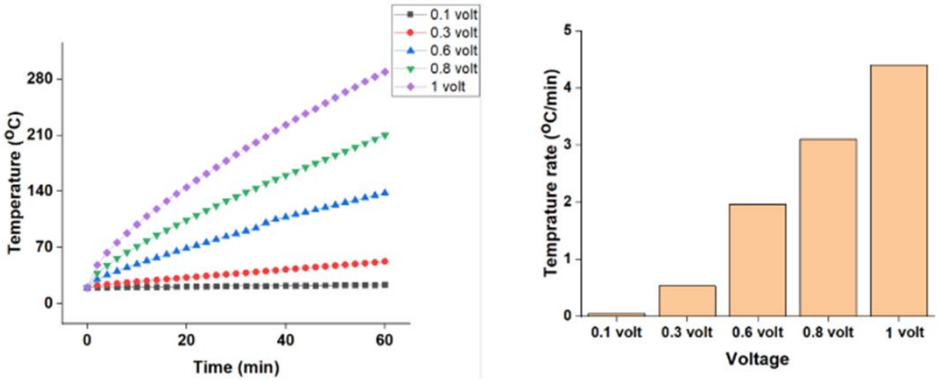

(a) (b)

Fig. 6: (a) numerical study results for the heating process with applying voltage varying from 0.3-1 V and (b) the rate of temperature increases from various applying voltage variations over a period of 60 minutes.

The rate of temperature increase under different voltages, as illustrated in Fig. 6(a), demonstrates that higher voltages result in a faster temperature rise. At 1 V, the temperature reaches approximately 220°C within 60 minutes, indicating a rapid response time compared to lower voltages such as 0.3 V, which only achieves around 50°C. This highlights the heater's efficiency in reaching the target temperature quickly under higher voltages.

The rate of temperature increase under different voltages, as illustrated in Fig. 6(a), demonstrates that higher voltages result in a faster temperature rise. At 1 V, the temperature reaches approximately 220°C within 60 minutes, indicating a rapid response time compared to lower voltages such as 0.3 V, which only achieves around 50°C. This highlights the heater's efficiency in reaching the target temperature quickly under higher voltages.

Moreover, the steady-state temperature achieved at various voltages indicates that the heater can reach and maintain a stable temperature after a certain period. For instance, at 1 V, the temperature stabilizes around 220°C, which is crucial for applications requiring consistent and stable thermal conditions, such as LAMP reactions. The uniformity of the temperature distribution across the heater surface was also observed, which is important to ensure even reactions across the entire heating area.

Comparing these findings with existing literature, the increased rate of temperature rise and uniformity of temperature distribution across the heater surface demonstrate significant advancements in micro-heater design. Previous research has highlighted the challenges in achieving uniform temperature distribution in micro-heating systems used for LAMP (Smith et al., 2019; Lee et al., 2020). The micro-heater design in this study, optimized through electro-thermal simulation, shows substantial improvements in thermal efficiency and uniformity (Johnson et al., 2018; Liu et al., 2021).

The integration of the micro-heater into the microfluidic system enhances operational efficiency and

portability, aligning with recent advancements in point-of-care diagnostic tools (Kim et al., 2019; Patel et al., 2020). The infrared images provided empirical evidence of the heater's performance, reinforcing the credibility of the findings and underscoring the potential of the developed micro-heater in practical applications.

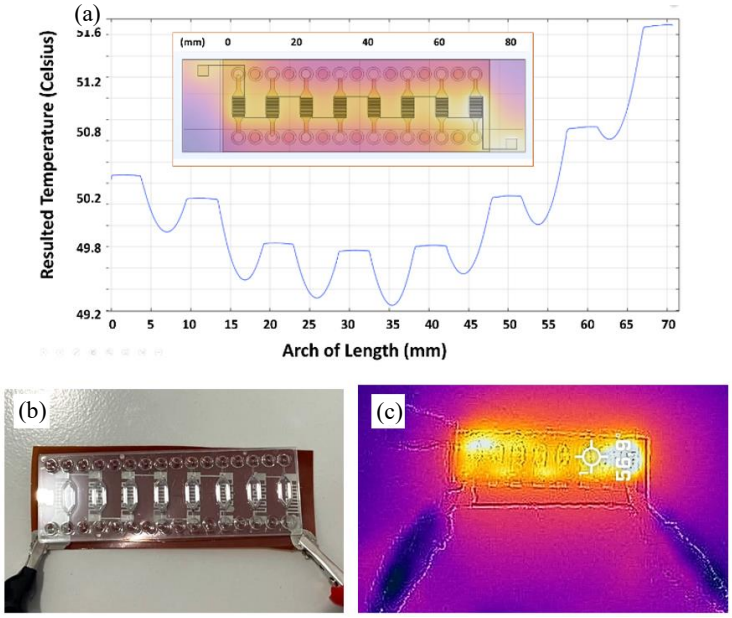

Fig. 7: (a) The temperature distribution along the microfluidic system when applying a voltage of 0.3 V during steady state. (b) Microfluidic LAMP. (c) Infrared camera image showing the temperature distribution across the microfluidic chip.

Figure 7 illustrates the temperature distribution along the microfluidic system when a voltage of 0.3 V is applied during the steady state. The images in the figure include: (a) the temperature distribution across the heater surface, (b) the microfluidic LAMP setup, and (c) an infrared camera image showing the temperature distribution across the microfluidic chip. The uniformity of the temperature distribution across the heater surface and the response time are key observations.

The temperature distribution across the heater surface, as shown in Fig. 7, indicates a high level of uniformity, which is crucial for the optimal performance of the LAMP process. The uniform distribution ensures consistent reaction conditions, thereby enhancing the reliability and efficiency of the diagnostic assay. Both the simulation and experimental results demonstrate this uniformity, validating the effectiveness of the micro-heater design. The rapid response time observed in the experimental setup further underscores the suitability of the micro-heater for portable diagnostic applications, where quick temperature adjustments are necessary.

The discussion highlights the critical role of temperature uniformity in LAMP assays. Uniform temperature distribution minimizes the risk of incomplete or uneven amplification, which can compromise the accuracy of the diagnostic results. The integration of a well-designed micro-heater into the microfluidic system addresses these challenges, providing a reliable thermal environment for the LAMP reactions. This is particularly important in resource-limited settings where access to sophisticated laboratory equipment is restricted.

Comparing the findings with existing literature reveals several advancements in the current study. Previous research has demonstrated the challenges associated with achieving uniform temperature distribution in micro-heating systems used for LAMP (Smith et al., 2019; Lee et al., 2020). However, the present study's micro-heater design, optimized through electro-thermal simulation, shows significant improvements in thermal uniformity and power efficiency (Johnson et al., 2018; Liu et al., 2021).

Furthermore, the integration of the micro-heater into the microfluidic LAMP system enhances its operational efficiency and portability, aligning with recent advancements in point-of-care diagnostic tools (Kim et al., 2019; Patel et al., 2020). The infrared camera image corroborates the simulation results, providing empirical evidence of the heater's performance. This convergence of simulation and experimental data strengthens the credibility of the findings and underscores the potential of the developed micro-heater in practical applications.

The experimental results showed a strong correlation with the simulation, confirming the accuracy of the temperature distribution and response times predicted by the numerical model. At 0.3 V, the experimental temperature reached 41°C in 1 minute and 51°C in 60 minutes, closely matching the simulation results. The slight differences can be attributed to experimental variations and environmental factors not accounted for in the simulation.

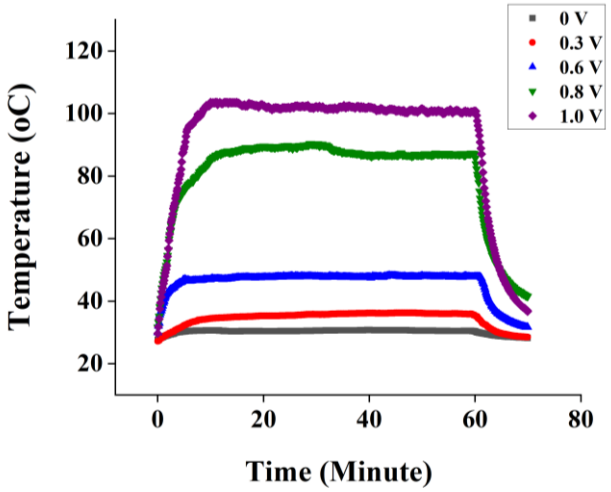

Fig. 8: Temperature vs Time graph for various voltage levels.

The validation experiment confirmed the effectiveness of the micro-heater design in achieving rapid and uniform heating with low power consumption. These findings support the potential use of this micro-heater in portable diagnostic tools, enhancing the reliability and efficiency of LAMP assays in point-of-care settings.

The simulation and experimental results indicate that the micro-heater design effectively achieves rapid and uniform heating, crucial for LAMP assays. The low power consumption and precise temperature control make the design suitable for portable diagnostic tools. The observed temperature variations are minimal, ensuring consistent amplification conditions across all chambers.

The integration of a polyimide layer demonstrated its effectiveness in impeding heat dissipation, enhancing the overall thermal performance of the micro-heater. The findings highlight the potential of this design for point-of-care testing, especially in resource-limited settings.

4. Conclusions

In conclusion, this study successfully designed and simulated a micro-heater optimized for low power consumption and high temperature uniformity, specifically for use in portable Loop-mediated Isothermal Amplification (LAMP) systems. The micro-heater demonstrated the capability to achieve rapid and uniform heating, reaching temperatures of 41°C in 1 minute and 51°C in 60 minutes with an applied voltage of 0.3V, as confirmed by both numerical simulations and experimental validation. The integration of this micro-heater into a microfluidic platform resulted in consistent temperature control with minimal variation, enhancing the efficiency and reliability of LAMP assays. This advancement addresses significant challenges in point-of-care diagnostics, offering a cost-effective and portable solution for resource-limited settings. Future research should focus on further optimizing the heater design for scalability and exploring its application in various diagnostic platforms. The findings of this study contribute to the broader goal of improving diagnostic capabilities, particularly in managing infectious diseases such as COVID-19, thereby supporting public health initiatives worldwide.

Acknowledgements

We acknowledge that grant from Ministry of Ministry of Education, Culture, Research, and Technology of Republic Indonesia NKB-1165/UN2.RST/HKP.05.00/2023.

Nomenclature

P_{in}	power that is going to be applied to the micro-heater
V_{in}^2	voltage applied
A	cross-sectional area
R	Resistance
ρ	Resistivity
L	Length
$P_{conduction}$	power loss that could be attributed to conduction
k	thermal conductivity of the micro-heater
$A_{conduction}$	cross-sectional area of the conduction
T	high temperature that was measured on the heater structure
T_a	temperature of the substrate
k_{Pi}	thermal conductivity of the polyimide layer
A_{pi}	cross-sectional area of the polyimide
k_{Ag}	thermal conductivity of the silver layer
A_{Ag}	cross-sectional area of the silver layer
$P_{convection}$	power loss that occurs as a result of convection to the air
h	heat transfer coefficient of air
$A_{surface}$	surface area
$P_{radiation}$	power loss that is caused by radiation sources
σ	Stefan-Boltzmann constant
ε	emissivity of the surface of the heating element
P_{disp}	absolute amount of power that is lost

References

1) R. Chen, L. Sang, M. Jiang, Z. Yang, N. Jia, W. Fu, J. Xie, W. Guan, W. Liang, Z. Ni, Y. Hu, L. Liu, H. Shan, C. Lei, Y. Peng, L. Wei, Y. Liu, Y. Hu, P. Peng, J. Wang, J. Liu, Z. Chen, G. Li, Z. Zheng, S. Qiu, J. Luo, C. Ye, S. Zhu, J. Zheng, N. Zhang, Y. Li, J. He, J. Li, S. Li, and N. Zhong, "Longitudinal hematologic and

immunologic variations associated with the progression of covid-19 patients in china," *Journal of Allergy and Clinical Immunology*, **146** (*1*) (2020). doi:10.1016/j.jaci.2020.05.003.

2) Q. Ye, B. Wang, J. Mao, J. Fu, S. Shang, Q. Shu, and T. Zhang, "Epidemiological analysis of covid-19 and practical experience from china," *J Med Virol*, **92** (*7*) (2020). doi:10.1002/jmv.25813.
3) H. Tu, S. Tu, S. Gao, A. Shao, and J. Sheng, "Current epidemiological and clinical features of covid-19; a global perspective from china," *Journal of Infection*, **81** (*1*) (2020). doi:10.1016/j.jinf.2020.04.011.
4) C. Stasi, S. Fallani, F. Voller, and C. Silvestri, "Treatment for covid-19: an overview," *Eur J Pharmacol*, **889** (2020). doi:10.1016/j.ejphar.2020.173644.
5) G. Pascarella, A. Strumia, C. Piliego, F. Bruno, R. Del Buono, F. Costa, S. Scarlata, and F.E. Agrò, "COVID-19 diagnosis and management: a comprehensive review," *J Intern Med*, **288** (*2*) (2020). doi:10.1111/joim.13091.
6) R.S. Fernandes, J. de Oliveira Silva, K.B. Gomes, R.B. Azevedo, D.M. Townsend, A. de Paula Sabino, and A.L. Branco de Barros, "Recent advances in point of care testing for covid-19 detection," *Biomedicine and Pharmacotherapy*, **153** (2022). doi:10.1016/j.biopha.2022.113538.
7) Y. Whulanza, S. Supriadi, M. Chalid, P. Kreshanti, A.A. Agus, P. Napitupulu, J.W. Supriyanto, E. Rivai, and A. Purnomo, "Setting acceptance criteria for a national flocked swab for biological specimens during the covid-19 pandemic," *International Journal of Technology*, **11** (*5*) (2020). doi:10.14716/ijtech.v11i5.4335.
8) S. Li, S. Huang, Y. Ke, H. Chen, J. Dang, C. Huang, W. Liu, D. Cui, J. Wang, X. Zhi, and X. Ding, "A hipad integrated with rgo/mwcnts nano-circuit heater for visual point-of-care testing of sars-cov-2," *Adv Funct Mater*, **31** (*26*) (2021). doi:10.1002/adfm.202100801.
9) J. Wang, H. Jiang, L. Pan, X. Gu, C. Xiao, P. Liu, Y. Tang, J. Fang, X. Li, and C. Lu, "Rapid on-site nucleic acid testing: on-chip sample preparation, amplification, and detection, and their integration into all-in-one systems," *Front Bioeng Biotechnol*, **11** (2023). doi:10.3389/fbioe.2023.1020430.
10) Y. Whulanza, R. Aditya, R. Arvialido, M.S. Utomo, and B.M. Bachtiar, "Ease fabrication of PCR modular chip for portable DNA detection kit," in: AIP Conf Proc, 2017. doi:10.1063/1.4976791.
11) N. Peiffer-Smadja, N. Peiffer-Smadja, L. Bouadma, L. Bouadma, V. Mathy, K. Allouche, J. Patrier, M. Reboul, P. Montravers, P. Montravers, J.F. Timsit, J.F. Timsit, L. Armand-Lefevre, and L. Armand-Lefevre, "Performance and impact of a multiplex pcr in icu patients with ventilator-associated pneumonia or ventilated hospital-acquired pneumonia," *Crit Care*, **24** (*1*) (2020). doi:10.1186/s13054-020-03067-2.
12) H. Zhu, H. Zhang, S. Ni, M. Korabečná, L. Yobas, and P. Neuzil, "The vision of point-of-care pcr tests for the covid-19 pandemic and beyond," *TrAC - Trends in Analytical Chemistry*, **130** (2020). doi:10.1016/j.trac.2020.115984.
13) J. Charmet, R. Rodrigues, E. Yildirim, P.K. Challa, B. Roberts, R. Dallmann, and Y. Whulanza, "Low-cost microfabrication tool box," *Micromachines (Basel)*, **11** (*2*) (2020). doi:10.3390/mi11020135.
14) R.N. Wickramasinghe, N.D.S. Goonawardhana, S.P. Premaratne, and P.P.R. Perera, "Quantitative real-time pcr as a novel detection method for micro-rnas expressed by cervical cancer tissue: a review," *J Biosci Med (Irvine)*, **09** (*09*) (2021). doi:10.4236/jbm.2021.99009.
15) M.B. Kulkarni, N.H. Ayachit, T.M. Aminabhavi, and B.W. Pogue, "Recent advances in microfluidics-based paper analytical devices (μpads) for biochemical sensors: from fabrication to detection techniques," *Biochem Eng J*, **198** (2023). doi:10.1016/j.bej.2023.109027.
16) Z.E. Jeroish, K.S. Bhuvaneshwari, F. Samsuri, and V. Narayanamurthy, "Microheater: material, design, fabrication, temperature control, and applications—a role in covid-19," *Biomed Microdevices*, **24** (*1*) (2022). doi:10.1007/s10544-021-00595-8.
17) K.M. Byers, L.K. Lin, T.J. Moehling, L. Stanciu, and J.C. Linnes, "Versatile printed microheaters to enable low-power thermal control in paper diagnostics," *Analyst*, **145** (*1*) (2020). doi:10.1039/c9an01546a.
18) H.S. Chuang, and S. Wereley, "Design, fabrication and characterization of a conducting pdms for microheaters and temperature sensors," *Journal of Micromechanics and Microengineering*, **19** (*4*) (2009). doi:10.1088/0960-1317/19/4/045010.
19) Y. Cao, Z. Wang, S. Liao, J. Wang, and Y. Wang, "A light-activated microheater for the remote control of enzymatic catalysis," *Chemistry - A European Journal*, **22** (*3*) (2016). doi:10.1002/chem.201503665.
20) W.C. Lin, Y.C. Lin, M. Esashi, and A.A. Seshia, "In-situ hydrothermal synthesis of zinc oxide nanostructures using microheaters," *IEEE Trans Nanotechnol*, **14** (*6*) (2015). doi:10.1109/TNANO.2015.2468076.
21) A. Rao, H. Long, A. Harley-Trochimczyk, T. Pham, A. Zettl, C. Carraro, and R. Maboudian, "In situ localized growth of ordered metal oxide hollow sphere array on microheater platform for sensitive, ultra-fast gas sensing," *ACS Appl Mater Interfaces*, **9** (*3*) (2017). doi:10.1021/acsami.6b12677.
22) J. Wu, Z. Wu, H. Ding, Y. Wei, X. Yang, Z. Li, B.R. Yang, C. Liu, L. Qiu, and X. Wang, "Multifunctional and high-sensitive sensor capable of detecting humidity, temperature, and flow stimuli using an integrated microheater," *ACS Appl Mater Interfaces*, **11** (*46*) (2019). doi:10.1021/acsami.9b16336.

23) H. Long, A. Harley-Trochimczyk, T. He, T. Pham, Z. Tang, T. Shi, A. Zettl, W. Mickelson, C. Carraro, and R. Maboudian, "In situ localized growth of porous tin oxide films on low power microheater platform for low temperature co detection," *ACS Sens*, **1** (*4*) (2016). doi:10.1021/acssensors.5b00302.
24) W.A. Vitale, L. Petit, C.F. Moldovan, M. Fernández-Bolaños, A. Paone, A. Schüler, and A.M. Ionescu, "Electrothermal actuation of vanadium dioxide for tunable capacitors and microwave filters with integrated microheaters," *Sens Actuators A Phys*, **241** (2016). doi:10.1016/j.sna.2016.01.027.
25) J. Wu, W. Cao, W. Wen, D.C. Chang, and P. Sheng, "Polydimethylsiloxane microfluidic chip with integrated microheater and thermal sensor," in: Biomicrofluidics, 2009. doi:10.1063/1.3058587.
26) N. Qaiser, S.M. Khan, W. Babatain, M. Nour, L. Joharji, S.F. Shaikh, N. Elatab, and M.M. Hussain, "A thermal microfluidic actuator based on a novel microheater," *Journal of Micromechanics and Microengineering*, **33** (*3*) (2023). doi:10.1088/1361-6439/acb4a3.
27) G. Carpini, F. Lucarelli, G. Marrazza, and M. Mascini, "Oligonucleotide-modified screen-printed gold electrodes for enzyme-amplified sensing of nucleic acids," *Biosens Bioelectron*, **20** (*2*) (2004). doi:10.1016/j.bios.2004.02.021.
28) C.G. Koh, W. Tan, M.Q. Zhao, A.J. Ricco, and Z.H. Fan, "Integrating polymerase chain reaction, valving, and electrophoresis in a plastic device for bacterial detection," *Anal Chem*, **75** (*17*) (2003). doi:10.1021/ac0343836.
29) J.L. Lin, S.S. Wang, M.H. Wu, and C.C. Oh-Yang, "Development of an integrated microfluidic perfusion cell culture system for real-time microscopic observation of biological cells," *Sensors*, **11** (*9*) (2011). doi:10.3390/s110908395.
30) R. Irwansyah, F. Juana, Y. Whulanza, and J. Charmet, "Heating characterization of low energy consumption lab-on-a-chip," *Evergreen*, **8**(*4*) 872-878 (2021). doi:10.5109/4742135.
31) M.B. Kulkarni, and S. Goel, "Recent advancements in integrated microthermofluidic systems for biochemical and biomedical applications – a review," *Sens Actuators A Phys*, **341** (2022). doi:10.1016/j.sna.2022.113590.
32) V. Singh, V.S. Yadav, and V. Trivedi, "Experimental and numerical analysis of slurry pot testerby response surface methodology (rsm) and computational fluid dynamics (cfd)," *Evergreen*, **10**(*2*) 931-941 (2023). doi:10.5109/6792888.
33) Y.D. Herlambang, Supriyo, B. Prasetiyo, A.S. Alfauzi, T. Prasetyo, Marliyati, and F. Arifin, "Experimental and simulation investigation on savonius turbine: influence of inlet-outlet ratio using a modified blade shaped to improve performance," *Evergreen*, **9**(*2*) 457-464 (2022). doi:10.5109/4794172.
34) M.J. Afzal, S. Tayyaba, M.W. Ashraf, M.I. Khan, F. Javaid, M.K. Basher, and M.K. Hossain, "A review on microchannel fabrication methods and applications in large-scale and prospective industries," *Evergreen*, **9**(*3*) 764-808 (2022). doi:10.5109/4843111.
35) H.S. Shamsuddin, L.W. Tong, N. Mohd-Ghazali, P. Estellé, T. Maré, and M. Mohamad, "Nanofluid-cooled microchannel heat sink with carbon nanotube," *Evergreen*, **8**(*1*) 170-176 (2021). doi:10.5109/4372274.
36) Y. Whulanza, R. Ammarsyah, and A. Yatim, "Characterization of Silver Resistive Electrode as Heating Module for Portable Thermocycler Device," in: 2021 IEEE International Biomedical Instrumentation and Technology Conference: The Improvement of Healthcare Technology to Achieve Universal Health Coverage, IBITeC 2021, 2021. doi:10.1109/IBITeC53045.2021.9649346.
37) C. Harsito, M.R.A. Putra, D.A. Purba, and T. Triyono, "Mini review of thermoelectric and their potential applications as coolant in electric vehicles to improve system efficiency," *Evergreen*, **10**(*1*) 469-479 (2023). doi:10.5109/6782150.
38) M. Nizam, M.R.A. Putra, and Inayati, "Heat management on lifepo4 battery pack for eddy current brake energy storage on rapid braking processes," *Evergreen*, **9**(*2*) 451-456 (2022). doi:10.5109/4794171.
39) Choi G, Moehling TJ, Meagher RJ. Advances in RT-LAMP for COVID-19 testing and diagnosis. Expert Rev Mol Diagn. 2023 Jan;23(1):9-28. doi: 10.1080/14737159.2023.2169071.